Characteristic Melting Behavior of Double Crystalline Poly(ϵ-caprolactone)-*block*-polyethylene Copolymers

Shuichi Nojima,* Toshimitsu Kiji, and Yuya Ohguma

Department of Organic and Polymeric Materials, Graduate School of Science and Engineering, Tokyo Institute of Technology, H-125, 2-12-1 Ookayama, Meguro-Ku, Tokyo 152-8552, Japan

Received December 5, 2006; Revised Manuscript Received July 23, 2007

ABSTRACT: The melting behavior of double crystalline poly(ϵ-caprolactone)-*block*-polyethylene (PCL-*b*-PE) copolymers, crystallized at various temperatures T_c below the melting point of both blocks, has been investigated by time-resolved small-angle X-ray scattering with synchrotron radiation (SR−SAXS), conventional wide-angle X-ray diffraction (WAXD), and differential scanning calorimetry (DSC). The melting temperature of PCL blocks $T_{m,PCL}$ was ca. 56 °C and that of PE blocks $T_{m,PE}$ was ca. 96 °C, so that the PCL blocks melted first during heating followed by the melting of PE blocks. This melting behavior was unique when compared with that of crystalline homopolymers and crystalline−amorphous diblock copolymers. That is, the long period (LP) of the lamellar morphology, an alternating structure consisting of thin crystals and amorphous layers, decreased considerably at $T_{m,PCL}$ for PCL-*b*-PE crystallized at every T_c investigated (22 °C < T_c < 50 °C). Upon further heating from $T_{m,PCL}$, LP decreased gradually for PCL-*b*-PE crystallized at higher T_c (>40 °C) (h-PCL-*b*-PE) while it was constant for PCL-*b*-PE crystallized at lower T_c (<40 °C). The morphology appearing in h-PCL-*b*-PE between $T_{m,PCL}$ and $T_{m,PE}$ was metastable, and the gradual decrease in LP during heating originated from the continuous rearrangement of the PE lamellar morphology facilitated by the melting of thinner PE crystals, which were previously formed by the crystallization of PCL blocks at T_c.

1. Introduction

The crystallization behavior of double crystalline block copolymers is extremely complicated depending on the molecular characteristics, in particular, the melting temperature T_m of constituent blocks.[1] When T_m values of two different blocks are close enough we can expect a simultaneous crystallization of both the blocks by quenching from a microphase-separated melt into low temperatures to yield an interesting morphology that is never observed in binary crystalline/crystalline polymer blends. This is the case for the di- and triblock copolymers consisting of poly(ethylene oxide) (PEO) and poly(ϵ-caprolactone) (PCL), and several studies are reported for the unique crystallization behavior and resulting morphology.[2−9] On the other hand, when T_m of one block is sufficiently higher than that of the other, we have a different story; that is, we expect a separate crystallization of two blocks, where the higher-T_m blocks crystallize first to yield a crystallized lamellar morphology and subsequently the lower-T_m blocks crystallize starting from this lamellar morphology. There are also some studies on the crystallization behavior for such double crystalline copolymers.[10−26]

We have recently investigated the crystallization behavior and resulting morphology of PCL-*block*-polyethylene (PCL-*b*-PE) copolymers,[21,22] where T_m of the PCL blocks $T_{m,PCL}$ was ca. 56 °C and that of PE blocks $T_{m,PE}$ 96 °C, and found that the crystallization behavior was greatly influenced by the crystallization temperature T_c. As a result, the final morphology after the crystallization of PCL blocks also depended significantly on T_c; at lower T_c (<35 °C), the PCL blocks crystallized within the pre-existing PE lamellar morphology (i.e., an alternating structure of thin PE crystals and amorphous layers) as a template while at higher T_c (>38 °C), the PE lamellar morphology was distorted or partially destroyed by the crystallization of PCL blocks to yield a new morphology more favorable for PCL crystallization. Therefore, the melting behavior of PCL-*b*-PE is expected to be intimately dependent on T_c because the starting morphology is significantly different.

The melting behavior of crystalline homopolymers has extensively been investigated so far,[27−30] and much information is available on the detailed morphological change during heating. It is well-known from these studies that lamella thickening occurs during heating to yield a steady increase of the long period (LP), the sum of thin crystal thickness and amorphous layer thickness, of the lamellar morphology. We have previously investigated the melting behavior of crystalline−amorphous diblock copolymers, PCL-*block*-polybutadiene (PCL-*b*-PB), and found that LP did not change at all during heating up to $T_{m,PCL}$.[31,32] This is because the crystallized lamellar morphology is controlled by a delicate balance between PCL lamellar crystals and amorphous PB layers; that is, the thickening of PCL lamellae brings about a free energy penalty for the conformation of amorphous PB blocks. We concluded from these studies that the melting behavior of crystalline−amorphous diblock copolymers was substantially different from that of crystalline homopolymers.

In this study, we investigate the melting behavior of double crystalline diblock copolymers, PCL-*b*-PE, where the starting morphology depends significantly on T_c, and therefore, we expect T_c-dependent melting behavior during heating. This is the motivation of this study, and we try to explain the characteristic melting behavior of PCL-*b*-PE mainly observed by time-resolved small-angle X-ray scattering with synchrotron radiation (SR−SAXS) from the viewpoint of the unique morphology formed in crystalline−crystalline diblock copolymers.

2. Experimental Section

2.1. Materials. The samples used in this study are double crystalline PCL-*b*-PE diblock copolymers, which were obtained by

* Corresponding author. Telephone:+81-3-5734-2132. Fax: +81-3-5734-2888. E-mail: snojima@polymer.titech.ac.jp.

10.1021/ma0627830 CCC: $37.00
Published on Web 09/18/2007

Table 1

	M_n[a]	M_n/M_w[b]	PCL:PE[c] (vol %)	EB[c] (mol %)	$T_{m,PCL}$[d] (°C)	$T_{m,PE}$[d] (°C)
A2	11000	1.09	69:31	6	55	97
A3	18000	1.18	51:49	5	56	95

[a] Determined by membrane osmometry. [b] Determined by GPC. [c] Determined by 1H NMR (EB: ethyl branch). [d] Determined by DSC for the samples crystallized at room temperature.

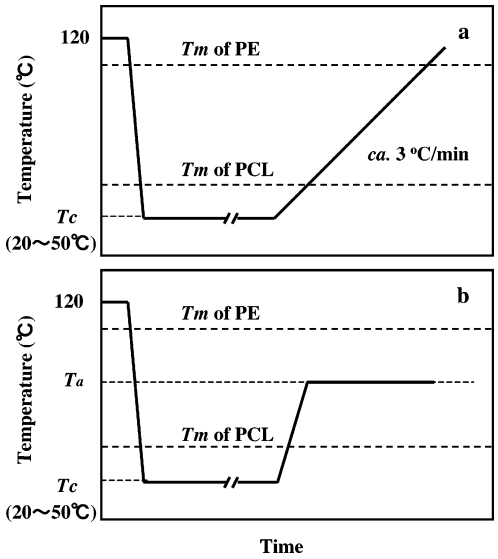

Figure 1. Thermal history applied to the sample: (a) heating at a constant rate (ca. 3 °C/min) from T_c up to $T_{m,PE}$ and (b) annealing at T_a between $T_{m,PCL}$ and $T_{m,PE}$.

the hydrogenation of PCL-*b*-PB diblocks anionically synthesized under vacuum. The methods of PCL-*b*-PB synthesis and the subsequent hydrogenation were already reported.[21,22,33,34] We used two PCL-*b*-PE copolymers (designated by A2 and A3) in this study to check the generality of melting behavior observed, and their molecular characteristics are shown in Table 1. Both copolymers contain a small amount of ethyl branch (EB). This EB yielded a broad melting range of PE blocks with the significant reduction of crystallinity and melting temperature (comparable with the literature values for model polyethylenes with various branch contents[35]), and therefore the resulting PE lamellar morphology may have a different degree of confinement for the subsequent crystallization of PCL blocks when compared with the case of linear polyethylenes. The crystallization behavior and resulting morphology of A2 and A3 were already reported,[21,22] and they depended intimately on the crystallization temperature T_c; at lower T_c (<35 °C) the PCL block crystallized within the existing PE lamellar morphology as a template while at higher T_c (>38 °C) it crystallized by distorting and/or partially destroying the PE lamellar morphology.

The melting temperature of PCL blocks $T_{m,PCL}$ is ca. 56 °C and that of PE blocks $T_{m,PE}$ is ca. 96 °C, so that the PCL block melts first during heating to reproduce the PE lamellar morphology followed by the melting of PE blocks at a high-temperature range (∼100 °C). Therefore, we can expect a T_c-dependent *restoration* of the deformed PE lamellar morphology just after the melting of PCL blocks, because the degree of deformation is highly influenced by T_c, as mentioned above.

2.2. Thermal History Applied to the Samples. We used two kinds of thermal history to observe the melting behavior of PCL-*b*-PE by SR−SAXS, which are shown in Figure 1. The order−disorder transition temperature (ODT) of microdomain structure is above 120 °C for both samples, but the starting morphology at 120 °C (microdomain structure) is completely replaced with the PE lamellar morphology during quenching, from which the PCL block starts to crystallize.[22]

In first thermal history (Figure 1a), the sample crystallized at T_c for a long time was heated at a constant rate (ca. 3 °C/min) and the SR−SAXS measurement was made until PE blocks completely melted (i.e., up to 120 °C). In second thermal history (Figure 1b), the sample crystallized at T_c was quickly transferred to a high-temperature T_a between $T_{m,PCL}$ and $T_{m,PE}$ and annealed at T_a, where PCL blocks melted completely while PE blocks still crystallized, so that the recovery process of the deformed PE lamellar morphology was expected during annealing. The SR−SAXS measurement was continued until the scattering curve did not change any more.

2.3. Differential Scanning Calorimetry (DSC) Measurements. A Perkin-Elmer DSC Pyris I was used with a heating rate of 10 °C/min to obtain $T_{m,PE}$ and $T_{m,PCL}$ and also crystallinity of each block (χ_{PE} and χ_{PCL}) for A2 and A3 crystallized at various T_c ranging from 5 to 50 °C. In addition, the change in χ_{PE} and χ_{PCL} against crystallization time t_c was obtained for A2 crystallized at $T_c = 25$ °C (where both PCL and PE blocks crystallized) to investigate the possibility of the residual (or secondary) crystallization of both blocks over a long time. The melting temperature was defined as the temperature at which the endothermic peak was maximum and χ_i (i = PCL or PE) was calculated from the endothermic peak area ΔH_i by

$$\chi_i = \Delta H_i/(\Delta H_i^0 f_i) \quad (1)$$

where ΔH_i^0 is the heat of fusion for perfect PE crystals (=277 J/g[36]) or PCL crystals (=135 J/g[37]), and f_i is the weight fraction of each block in PCL-*b*-PE. The DSC exothermic curve during cooling at a rate of 10 °C/min was preliminary measured to estimate the crystallization temperature of each block, where the PE block crystallized at ca. 85 °C and the PCL block at ca. 35 °C. The temperature and area calibration was performed with indium (T_m = 156.6 °C) and *n*-octacosanol (T_m = 83.2 °C).

2.4. Wide-Angle X-ray Diffraction (WAXD) Measurements. WAXD measurements were performed by using a conventional equipment (RIGAKU NANO−Viewer) with an image-plate (IP) detector. The sample thickness was ca. 2 mm for all measurements and the distance between the sample and IP was ca. 80 mm. The 2D WAXD pattern obtained was circularly averaged and relative intensity was evaluated as a function of diffraction angle 2θ after the background correction. Characteristic diffracted intensities were finally obtained as a function of t_c to evaluate the change in the crystallinity of each block.

2.5. Time-Resolved SR—SAXS Measurements. The time-resolved SR−SAXS measurements during heating or annealing were performed at Photon Factory in high energy accelerator research organization, Tsukuba Japan, with a small-angle X-ray equipment for solution (SAXES) installed at beamline BL-10C. Details of the equipment and the instrumentation are described in our previous publications.[32,38] The scattered intensity was recorded with a one-dimensional position-sensitive proportional counter (PSPC). In addition, the incident beam intensity with wave length λ = 0.1488 nm was monitored at before and after the sample by two ionization chambers for the evaluation of the frame-by-frame transmission factor of samples and also for the correction of a minor decrease in intensity during measurements. The SR−SAXS curve measured was corrected for the background scattering and the absorption by samples, but not for the smearing effect because SAXES employed a point-focusing optics. The SAXS curve after multiplying the Lorentz factor (=$4\pi s^2$) was finally obtained as a function of s defined by $s = (2/\lambda) \sin \theta$, where 2θ is the scattering angle.

2.6. Analysis of SR—SAXS Curves. The SR−SAXS curve had an intensity peak arising from an alternating structure consisting of crystalline (PE or PE + PCL) lamellae and amorphous layers during heating and annealing. We obtained the long period (LP) of this structure, peak intensity, and full width at half-maximum (fwhm) of the peak as a function of temperature (for heating process) and annealing time (for annealing process).

We also obtained the temperature dependence of invariant $Q(T)$ during heating, which is defined by

$$Q(T) = \int_0^\infty s^2 I(s)\, ds \tag{2}$$

In our SR−SAXS study, however, the time-resolved SAXS curves were limited to a finite angle ($s < 0.3$ nm^{-1}) owing to the fixed geometry of the apparatus, so that the wider-angle intensity could not be experimentally obtained. When scattered data in the wide-angle region are not available, it is usual that the background scattering I_b is considered constant and the scattered intensity is approximated by Porod's law extrapolation expressed as

$$I(s)s^4 = \text{constant} + I_b s^4 \tag{3}$$

The slope in a plot of $I(s)s^4$ vs s^4 gives I_b arising from composition fluctuation.

$Q(T)$ contains information on the morphology during melting and can be expressed by a mean-square difference in the electron density $\langle\Delta\rho^2\rangle$ among different phases

$$Q(T) = k\langle\Delta\rho^2\rangle \tag{4}$$

where k is a constant relating to the X-ray irradiated volume. PCL-*b*-PE takes a microdomain structure at high temperatures ($> T_{m,PE}$), so that the system consists of two phases, i.e., amorphous PCL and PE phases. In this case $\langle\Delta\rho^2\rangle$ can be written as

$$\langle\Delta\rho^2\rangle = (\rho_{PE,a} - \rho_{PCL,a})^2 \phi_{PCL}(1 - \phi_{PCL}) \tag{5}$$

where ϕ_{PCL} is the volume fraction of PCL blocks in the system, and $\rho_{PE,a}$ and $\rho_{PCL,a}$ are the electron density of amorphous PE and PCL blocks, respectively, which can be evaluated from the temperature dependence of specific volume $v_{sp}(T)$. For amorphous PE[39]

$$v_{sp}(T) = 1.1696 + (1.77 \times 10^{-4})T \tag{6}$$

and for amorphous PCL,[37]

$$v_{sp}(T) = 0.9106 + (6.01 \times 10^{-4})T \tag{7}$$

where $v_{sp}(T)$ is in cm^3/g and T in °C.

At $T_{m,PE} > T > T_{m,PCL}$ the PE blocks crystallize and eventually the system has three phases, that is, PE crystal phase, amorphous PE phase, and amorphous PCL phase, if we assume that amorphous PE blocks segregate completely from amorphous PCL blocks with a sharp interface. In this case $\langle\Delta\rho^2\rangle$ can be conveniently expressed by the combination of two-phase systems, and given by[40]

$$\begin{aligned}\langle\Delta\rho^2\rangle = {} & (\rho_{PE,a} - \rho_{PCL,a})^2 \phi_{PCL}(1 - \phi_{PCL})(1 - \chi'_{PE}) + \\ & (\rho_{PE,a} - \rho_{PE,c})^2 (1 - \phi_{PCL})^2 \chi'_{PE}(1 - \chi'_{PE}) + \\ & (\rho_{PCL,a} - \rho_{PE,c})^2 \phi_{PCL}(1 - \phi_{PCL})\chi'_{PE}\end{aligned} \tag{8}$$

where $\rho_{PE,c}$ is the electron density of PE crystals, which can be evaluated by assuming that the specific volume of PE crystals is 1.00 cm^3/g irrespective of temperature,[41] and χ'_{PE} is the volume fraction of crystallized PE blocks against total PE blocks in the system. By substituting eqs 5 and 8 into eq 4, we can get χ'_{PE} as a function of temperature during heating.

3. Results and Discussion

3.1. Time-Resolved SR—SAXS Curves during Heating. Figure 2 shows the typical time-resolved SR−SAXS curves during heating at ca. 3 °C/min from 39 to 115 °C for A2 crystallized at 42 °C, where we can see a complicated change in the SAXS curves; the peak intensity I at $s \sim 0.04$ nm^{-1} decreases appreciably at $T_{m,PCL}$ followed by a gradual increase of I toward $T_{m,PE}$, and finally a couple of scattered peaks appear at $T_{m,PE}$, which arise from a microdomain structure formed in the melt. These changes in I can be successfully explained by considering the electron density of PCL crystals (=393 e/nm^3), PE crystals (=340 e/nm^3), amorphous PCL (=337 e/nm^3 at 100 °C), and amorphous PE (=289 e/nm^3 at 100 °C) at each temperature during heating. That is, the electron density contrast in the system considerably decreases by the melting of PCL crystals at $T_{m,PCL}$ to yield an appreciable decrease in I. I at $T_{m,PCL} < T < T_{m,PE}$, on the other hand, substantially arises from the contrast between amorphous PE ($\rho_{PE,a}$) and PE crystals + amorphous PCL ($\rho_{PE,c}$ or $\rho_{PCL,a}$) because the electron density of PE crystals is nearly equal to that of amorphous PCL. A small amount of PE crystals melts during heating, as we will discuss later, and the volume fraction of amorphous PE $\phi_{PE,a}$ (<0.5) gradually increases to yield the increase of I because I is roughly proportional to $\phi_{PE,a}(1 - \phi_{PE,a})(\rho_{PE,a} - \rho_{PE,c})^2$. We obtained qualitatively similar SR−SAXS curves for A2 and A3 crystallized at each T_c.

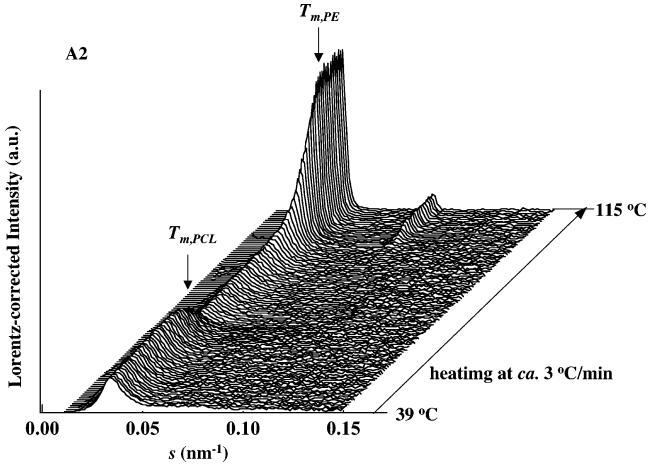

Figure 2. Typical time-resolved SR−SAXS curves during heating at ca. 3 °C/min from 39 to 115 °C for A2 crystallized at 42 °C for a long time.

Figure 3 shows the temperature dependence of LP (evaluated from the angular position of SAXS peaks) (a), peak intensity (b), full width at half-maximum (fwhm) of the peak (c), and invariant (d) for A2 crystallized at 23 °C (low T_c) and 48 °C (high T_c). We can find several important features characteristic of the melting in crystalline−crystalline diblock copolymers.

First, a considerable decrease in LP is observed at $T_{m,PCL}$ for PCL-*b*-PE crystallized both at high T_c and low T_c. The temperature at which the decrease of LP terminates exactly corresponds to the temperature at the minimum of peak intensity and invariant (dotted lines). Second, $T_{m,PCL}$ for PCL-*b*-PE crystallized at high T_c is significantly higher than that at low T_c but $T_{m,PE}$ is similar for both cases. The difference in $T_{m,PCL}$ for two cases reflects the difference in the crystallization mechanism and eventually the size of PCL crystals existing in the system. Furthermore, the temperature range of melting for PCL blocks is relatively narrow and that for PE blocks is wide (from $T^s_{m,PE}$ to $T^e_{m,PE}$, which are defined as flection points of LP in Figure 3a). These temperature ranges of melting for each block nearly correspond to those of the endothermic peaks observed by DSC (Figure 5a). Third, LP continues to decrease upon further heating from $T_{m,PCL}$ for PCL-*b*-PE crystallized at high T_c while it is almost constant for PCL-*b*-PE crystallized at low T_c until PE blocks start to melt at $T = T^s_{m,PE}$. In this temperature range (i.e., $T_{m,PCL} < T < T^s_{m,PE}$), the fwhm is also significantly different between the two cases, suggesting the difference in the regularity of PE lamellar morphology.

These differences extracted from SR−SAXS curves certainly originate from the morphological difference in PCL-*b*-PE

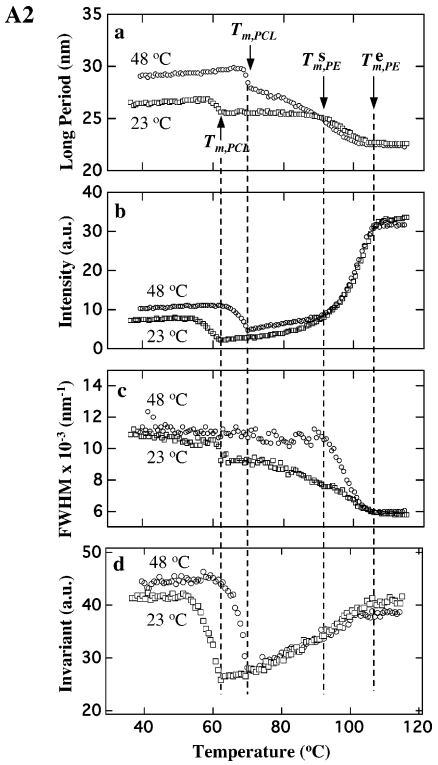

Figure 3. Long period (a), peak intensity (b), fwhm of the peak (c), and invariant (d) evaluated from the SR−SAXS curves plotted against temperature during heating for A2 crystallized at 48 (circle) and 23 °C (square).

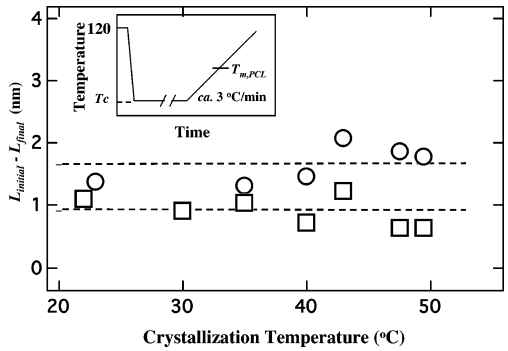

Figure 4. Difference in long period, $L_{initial} - L_{final}$, before and after the melting of PCL blocks plotted against T_c for A2 (circle) and A3 (square). The inset shows the thermal history applied to the sample.

crystallized at high T_c and low T_c. In this study, we devote our attention to (1) the considerable decrease in LP observed at $T_{m,PCL}$ and (2) the temperature dependence of LP (i.e., gradual decrease or no change depending on T_c) during heating ($T_{m,PCL} < T < T^s_{m,PE}$), and we mainly discuss these points.

3.2. Decrease in Long Period at $T_{m,PCL}$. Figure 4 shows the difference in LP, $L_{initial} - L_{final}$, before and after the melting of PCL blocks plotted against T_c for A2 (circle) and A3 (square), where it is almost constant irrespective of T_c but depends somewhat on the sample (A2 or A3). This indicates L_{final} is different from the initial LP of the PE lamellar morphology (L_{PE}); at $T_c < 35$ °C, L_{final} is significantly smaller than L_{PE}, and at $T_c > 35$ °C L_{final} is larger or smaller than L_{PE} depending on T_c. Therefore, the PE lamellar morphology appearing just after the melting of PCL blocks is not identical with that existing before the crystallization of PCL blocks. That is, the PE lamellar morphology changes substantially during the crystallization of PCL blocks at T_c.

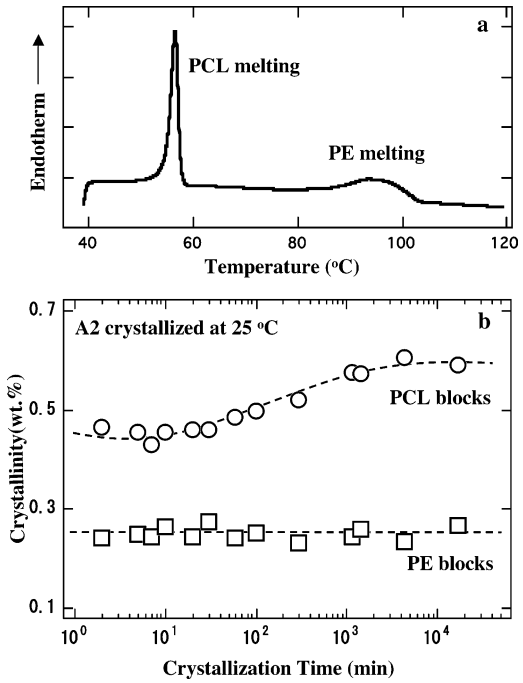

Figure 5. (a) Typical DSC curve during heating at 10 °C/min for A2 crystallized at 40 °C for 30 min. (b) The crystallization time dependence of χ_{PCL} (circle) and χ_{PE} (square) for A2 crystallized at 25 °C.

One of the possible reason for this change in the PE lamellar morphology may be the residual (or secondary) crystallization of PE and/or PCL blocks at T_c after the completion of the primary crystallization of PCL blocks, which is usually observed in crystalline homopolymers over a long period of time.[27] That is, this residual crystallization may yield a gradual change in the crystal shape of PCL and/or PE blocks, and once the PCL block melts completely at $T_{m,PCL}$, the deformed PE lamella remains and eventually the system takes more favorable morphology to reduce LP.

To verify the residual crystallization of each block at T_c over a long time, we measured the change in crystallinity of PE and PCL blocks at T_c as a function of crystallization time t_c by DSC and conventional WAXD techniques. Figure 5a shows a typical DSC thermogram during heating for A2 crystallized at 40 °C for 30 min, from which we evaluated the crystallinity of PE and PCL blocks, χ_{PE} and χ_{PCL}, separately. Figure 5b shows the t_c dependence of χ_{PE} (square) and χ_{PCL} (circle) for A2 crystallized at 25 °C, where χ_{PE} is nearly constant irrespective of t_c but χ_{PCL} increases steadily with increasing t_c, indicating that the PCL block crystallizes further after finishing the primary crystallization. This fact suggests the deformation of PE crystals, for example, partial melting and/or thinning of PE lamellae facilitated by the increase of χ_{PCL} because LP did not change during crystallization over a long time at T_c (which was verified by the conventional SAXS method).

The crystallization-induced melting was first reported by Hamley et al. for poly(L-lactide)-*block*-PCL (PLLA-*b*-PCL) diblock copolymers,[23,26] where the crystallization of PCL blocks yielded a partial melting of already crystallized PLLA blocks in order to compensate the space previously occupied by amorphous PCL blocks. The present DSC results do not clearly indicate the melting of PE blocks by the residual crystallization of PCL blocks, but it is also true that a small change in PE crystallinity is difficult to evaluate because the PE melting endotherm is diffuse and χ_{PE} contains much error than χ_{PCL}. If PE lamellae are partially transformed into thinner crystals by the residual crystallization of PCL blocks, the space on PE

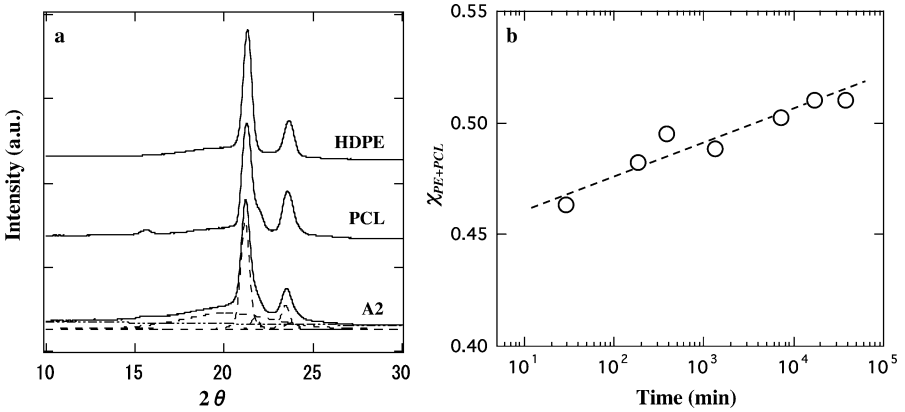

Figure 6. (a) WAXD patterns of crystallized PCL, high-density PE (HDPE), and A2. The WAXD curves for PCL and HDPE are shifted upward for legibility. (b) Crystallization time dependence of χ_{PE+PCL} for A2 crystallized at 25 °C.

lamellae available for the accommodation of amorphous PCL blocks increases compared with the case just before the crystallization of PCL blocks. Consequently, amorphous PCL blocks will approach to random-coil conformation after melting[42,43] to yield a moderate decrease in LP.

The DSC results may contain extra phenomena during heating, for example, recrystallization of PE blocks usually observed in crystalline homopolymers, which will smear the facts occurring during the residual crystallization of PCL blocks at T_c. Therefore, we complementarily employed WAXD method to investigate the change in χ_{PE} and χ_{PCL} during the long-time crystallization at T_c.

Figure 6a shows the typical WAXD curves from PCL homopolymer, high-density PE (HDPE), and PCL-*b*-PE (A2) crystallized at room temperature. Unfortunately the diffraction pattern from PE is almost identical with that from PCL,[44] so that it is impossible to evaluate χ_{PE} and χ_{PCL} separately, but the time dependence of combined crystallinity of PE and PCL blocks, χ_{PE+PCL}, can be obtained from the following equation,[45]

$$\chi_{PE+PCL} = \frac{\int_0^\infty s^2 I_c \, ds}{\int_0^\infty s^2 I_c \, ds + K\int_0^\infty s^2 I_a \, ds} \qquad (9)$$

where I_c is the major diffraction intensity located at $2\theta = 21°$ (110 reflection both for PCL and PE crystals), I_a the amorphous halo intensity, and K a constant expressing the ratio of diffraction efficiency between I_c and I_a and inherent in each crystallized block. Actually we decomposed the diffraction curves into several peaks (see Figure 6a, bottom) by a conventional computer program to obtain I_c. However I_c originated both from PE and PCL crystals and their volume ratio at t_c was unknown, so that it was impossible to calculate K from literature values of each component. Therefore, we simply put $K = 1$ in eq 9 and obtained t_c dependence of χ_{PE+PCL}. This means χ_{PE+PCL} is not the actual crystallinity of PE + PCL blocks, but it is only a measure for the change of PE + PCL crystallinity against t_c.

Figure 6b shows the plot of χ_{PE+PCL} against t_c, where χ_{PE+PCL} increases almost linearly with increasing t_c, indicating that the residual (or secondary) crystallization of PE and/or PCL blocks definitely occurs over a long period of time. From this fact, together with DSC results, we conclude that the residual (or secondary) crystallization of PCL blocks occurs after the primary crystallization of PCL blocks, and further increase of χ_{PCL} might induce the thinning of already crystallized PE lamellae, because total LP does not change during this process. At present, however, there is no direct evidence to show the relation between the residual crystallization of PCL blocks and the large reduction of LP just after the melting of PCL blocks.

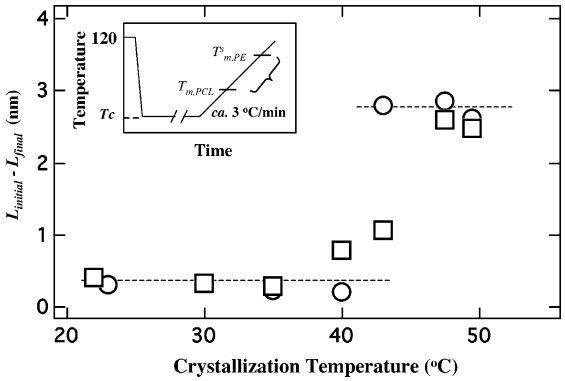

Figure 7. Change in long period, $L_{initial} - L_{final}$, during heating from $T_{m,PCL}$ to $T^s_{m,PE}$ plotted against T_c for A2 (circle) and A3 (square). The inset shows the thermal history applied to the sample.

3.3. Temperature Dependence of the Long Period between $T_{m,PCL}$ and $T^s_{m,PE}$. Figure 7 shows the change in LP, $L_{initial} - L_{final}$, during heating from $T_{m,PCL}$ to $T^s_{m,PE}$ plotted against T_c for A2 (circle) and A3 (square). Up to $T_c < 40$ °C, it is almost zero for both A2 and A3, indicating that LP does not change at all during heating ($T_{m,PCL} < T < T^s_{m,PE}$). This result is consistent with our previous observation during heating for semicrystalline PCL-*b*-PB copolymers.[32] On the other hand, when $T_c > 40$ °C the change is considerably large, which arises from the gradual decrease in LP during heating (Figure 3a). It may be a plausible reason that the scattering peak appearing at $T_{m,PCL} < T < T^s_{m,PE}$ is the superposition of those from the PE lamellar morphology (appearing at lower angle) and the microdomain structure (higher angle) and their ratio changes with increasing temperature to yield the gradual decrease of LP. However, this interpretation is not consistent with our experimental results. That is, we calculated the composite SAXS curves consisting of those from the PE lamellar morphology at 78 °C and the microdomain structure at 115 °C, and obtained the bimodal scattering peak at every ratio, i.e., two scattering peaks could not merge into one at any ratio. This is because two scattering peaks are extremely different in their position, shape, and intensity.

Figure 7 clearly indicates that the melting behavior at $T_{m,PCL} < T < T^s_{m,PE}$ relates intimately to T_c, that is, the difference in the starting morphology previously formed at T_c by the crystallization of PCL blocks. To elucidate the origin of this difference in the melting behavior between PCL-*b*-PE copolymers crystallized at low and high T_c, the temperature dependence

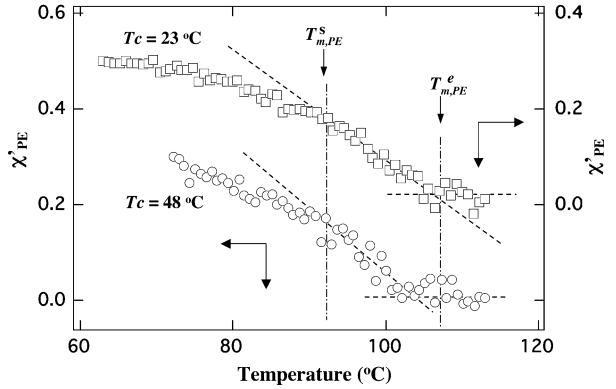

Figure 8. Temperature dependence of χ'_{PE} evaluated from $Q(T)$ for A2 crystallized at 48 °C (circle) and 23 °C (square).

of χ'_{PE} (eq 8) was evaluated from $Q(T)$ and plotted in Figure 8. χ'_{PE} decreases slightly with increasing temperature up to $T^s_{m,PE}$ followed by a steep decrease in the temperature region between $T^s_{m,PE}$ and $T^e_{m,PE}$ (dotted lines). Figure 8 implies that an appropriate amount of PE crystals melts little by little during heating even at $T_{m,PCL} < T < T^s_{m,PE}$. In addition, it is found from Figure 8 that the decrease in χ'_{PE} for PCL-*b*-PE crystallized at high T_c is slightly larger than that at low T_c in $T_{m,PCL} < T < T^s_{m,PE}$, suggesting that high-$T_c$ PCL-*b*-PE contains a larger amount of thin PE crystals and these crystals melt gradually during heating before reaching to $T^s_{m,PE}$. These thin crystals have been produced by the crystallization of PCL blocks at T_c, that is, the PE lamellar morphology was appreciably deformed or partially destroyed when PCL blocks crystallized at higher T_c to yield thin PE crystals. Therefore, it is concluded that the difference in the temperature dependence of χ'_{PE} between PCL-*b*-PE copolymers crystallized at high and low T_c shown in Figure 8 originates from the difference in the starting morphology after the crystallization of PCL blocks at each T_c.

It is interesting to investigate whether the morphology appearing during heating ($T_{m,PCL} < T < T^s_{m,PE}$) is stable or not. To get further information on this morphology we performed another time-resolved SR−SAXS experiments by using the thermal history shown in Figure 1b. That is, the sample, crystallized at T_c for a long time, was quickly transferred to a temperature T_a between $T_{m,PCL}$ and $T^s_{m,PE}$, and the morphological change at T_a was pursued by SR−SAXS. Figure 9a shows the plot of LP against annealing time t_a for A2 first crystallized at T_c = 45 (open circle) and 0 °C (closed circle) and subsequently moved to 70 °C, where t_a dependence of LP is extremely different between two cases; LP for A2 crystallized at 0 °C does not change at all during annealing, while that crystallized at 45 °C decreases considerably at the early stage of annealing and after that it keeps constant. The decrease of LP at the early stage of annealing suggests the transformation of the morphology formed at 45 °C into a new morphology favorable for PCL-*b*-PE at 70 °C.

The final LP is plotted against T_a in Figure 9b for A2 crystallized at 45 °C (closed circle) and 0 °C (closed square), where the change in LP during heating (Figure 3a) is also plotted (open symbols). LP finally obtained after annealing at T_a coincides moderately with that observed during heating for A2 crystallized both at high and low T_c, indicating that the morphology appearing during heating is not unstable but at least metastable depending on each temperature between $T_{m,PCL}$ and $T^s_{m,PE}$. That is, the morphology is successively rearranged during heating within a short time into the new morphology by the melting of thinner PE crystals, which leads to the conclusion

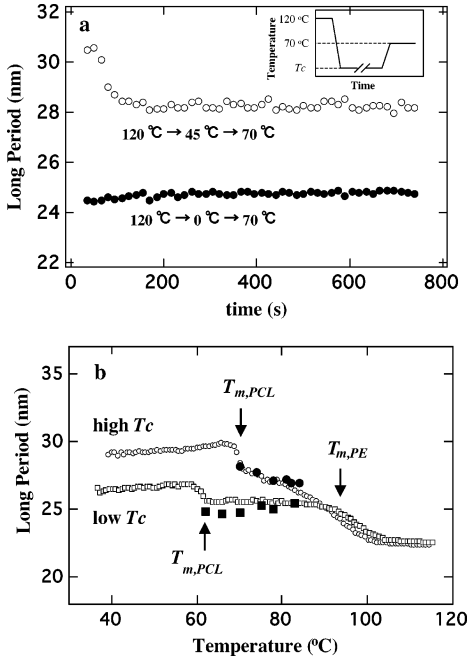

Figure 9. (a) Long period plotted against annealing time at 70 °C for A2 crystallized at 45 °C (open circle) and 0 °C (closed circle). The inset shows the thermal history applied to the sample in this case. (b) Final long period plotted against annealing temperature for A2 crystallized at high temperature (45 °C, closed circle) and low temperature (0 °C, closed square). Open symbols represent the temperature dependence of long period for A2 during heating at 3 °C/min (Figure 3a).

that the metastable morphology appearing at $T_{m,PCL} < T < T^s_{m,PE}$ is critically controlled both by T_c and T.

Next we evaluated the time necessary to achieve the metastable morphology at T_a by considering that this morphological rearrangement is a relaxation process from unstable into metastable state, and use the following equation to get the relaxation time τ of this process,

$$L(t_a) - L(\infty) = \{L(0) - L(\infty)\}\exp(-t_a/\tau) \qquad (10)$$

where $L(t_a)$ is LP at t_a, $L(\infty)$ the final LP, and τ the relaxation time of this process. A typical plot of $\ln\{L(t_a) - L(\infty)\}$ against t_a is shown in Figure 10a, and we can get τ from the slope. Figure 10b shows the T_a dependence of τ for A2 previously crystallized at 45 °C, where τ is almost constant (=27 s) irrespective of T_a, indicating that the morphological rearrangement occurs moderately fast compared with the heating rate employed in the heating studies (3 °C/min).

Conclusions

We have investigated the melting behavior of double crystalline diblock copolymers, poly(ϵ-caprolactone)-*block*-polyethylene (PCL-*b*-PE), crystallized at various temperatures T_c mainly by employing time-resolved small-angle X-ray scattering with synchrotron radiation (SR−SAXS). This melting behavior was unique and extremely different from that of crystalline homopolymers and also crystalline−amorphous diblock copolymers. The following conclusions were obtained from this study.

(1) The long period, an alternating distance of lamellar crystals and amorphous layers, decreased appreciably by the melting of PCL blocks for PCL-*b*-PE crystallized both at high and low T_c. The residual crystallization leads to the significant increase in PCL crystallinity, which might induce the deforma-

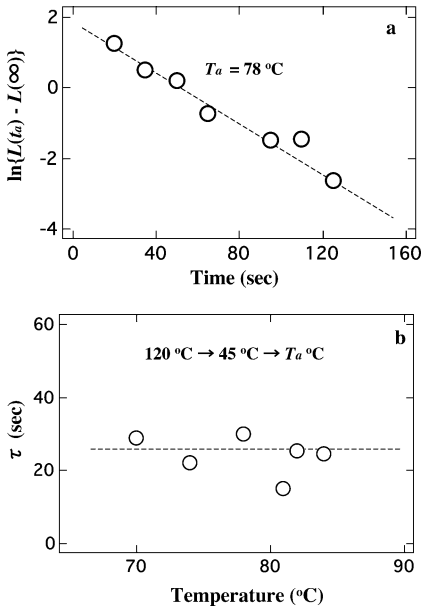

Figure 10. (a) Typical plot of $\ln\{L(t_a) - L(\infty)\}$ against annealing time t_a at 78 °C for A2. (b) Relaxation time τ plotted against annealing temperature T_a for A2 crystallized at 45 °C.

tion of already crystallized PE lamellae, for example, thinning of PE crystals. Therefore, the residual crystallization might be the reason for the considerable reduction of LP at $T_{m,PCL}$ because thinner PE lamellae have enough space on it to accommodate the amorphous PCL blocks, though we have no experimental result for this point.

(2) The long period continued to decrease on further heating after the melting of PCL blocks for PCL-*b*-PE crystallized at high T_c while it was almost constant for PCL-*b*-PE crystallized at low T_c. The morphology appearing at each temperature between $T_{m,PCL}$ and $T^s_{m,PE}$ was metastable, and controlled by the continuous melting of thin PE crystals, which had previously been formed by the crystallization of PCL blocks at T_c. As a result, the difference in the starting morphology formed by the crystallization of PCL blocks at low and high T_c is responsible for the difference in the melting behavior during heating at $T_{m,PCL} < T < T^s_{m,PE}$.

In summary, the melting behavior of double crystalline diblock copolymers is very complicated and many factors will influence this process, such as the crystallization temperature of low T_m blocks, resulting morphology at T_c, residual crystallization of both blocks at T_c, and so on. Therefore, more information is necessary to completely understand the melting behavior occurring in crystalline−crystalline diblock copolymers.

Acknowledgment. This work was supported in part by NEDO (New Energy and Industrial Technology Development Organization) launched in 2001 and also by Grants-in-Aid for Scientific Research on Basic Areas (B) (No. 17350102) from the Ministry of Education, Science, Sports, and Culture of Japan. The SR−SAXS measurement has been performed under the approval of Photon Factory Advisory Committee (No. 2006G078)

References and Notes

(1) Muller, A. J.; Arnal, M. L.; Balsamo, V. In *Lecture Notes in Physics 714*; Reiter, G., Strobl, G., Eds.; Springer-Verlag: Berlin, in press.
(2) Nojima, S.; Ono, M.; Ashida, T. *Polym. J.* **1992**, *24*, 1271.
(3) Gan, Z.; Jiang, B.; Zhang, J. *J. Appl. Polym. Sci.* **1996**, *59*, 961.
(4) Floudas, G.; Reiter, G.; Lambert, O.; Dumas, P. *Macromolecules* **1998**, *31*, 7279.
(5) Bogdanov, B.; Vidts, A.; Schacht, E.; Berghmans, H. *Macromolecules* **1999**, *32*, 726.
(6) Shiomi, T.; Imai, K.; Takenaka, K.; Takeshita, H.; Hayashi, H.; Tezuka, Y. *Polymer* **2001**, *42*, 3233.
(7) Jiang, S.; He, C.; An, L.; Chen, X.; Jiang, B. *Macromol. Chem. Phys.* **2004**, *205*, 2229.
(8) Sun, J.; Chen, X.; He, C.; Jing, X. *Macromolecules* **2006**, *39*, 3717.
(9) Takeshita, H.; Fukumoto, K.; Ohnishi, T.; Ohkubo, T.; Miya, M.; Takenaka, K.; Shiomi, T. *Polymer* **2006**, *47*, 8210.
(10) Kim, K. S.; Chung, S.; Chin, I. J.; Kim, M. N.; Yoon, J. S. *J. Appl. Polym. Sci.* **1999**, *72*, 341.
(11) Reiter, G.; Castelein, G.; Hoerner, P.; Riess, G.; Blumen, A.; Sommer, J. U. *Phys. Rev. Lett.* **1999**, *83*, 3844.
(12) Balsamo, V.; Paolini, Y.; Ronca, G.; Muller, A. J. *Macromol. Chem. Phys.* **2000**, *201*, 2711.
(13) Kim, J. K.; Park, D. J.; Lee, M. S.; Ihn, K. J. *Polymer* **2001**, *42*, 7429.
(14) Ueda, M.; Sakurai, K.; Okamoto, S.; Lohse, D. J.; MacKnight, W. J.; Shinkai, S.; Sakurai, S.; Nomura, S. *Polymer* **2003**, *44*, 6995.
(15) Albuerne, J.; Marquez, L.; Muller, A. J.; Raquez, J. M.; Degee, Ph.; Dubois, Ph.; Castelletto, V.; Hamley, I. W. *Macromolecules* **2003**, *36*, 1633.
(16) Ho, R. M.; Hsieh, P. Y.; Tseng, W. H.; Lin, C. C.; Huang, B. H.; Lotz, B. *Macromolecules* **2003**, *36*, 9085.
(17) Maglio, G.; Migliozzi, A.; Palumbo, R. *Polymer* **2003**, *44*, 369.
(18) Balsamo, V.; Gil, G.; Navarro, C. U.; Hamley, I. W.; Gyldenfeldt, F.; Abetz, V.; Canizales, E. *Macromolecules* **2003**, *36*, 4515.
(19) Sun, L.; Liu, Y.; Zhu, L.; Hsiao, B. S.; Avila-Orta, C. A. *Polymer* **2004**, *45*, 8181.
(20) Balsamo, V.; Urdaneta, N.; Perez, L.; Carrizales, P.; Abetz, V.; Muller, A. J. *Eur. Polym. J.* **2004**, *40*, 1033.
(21) Nojima, S.; Akutsu, Y.; Washino, A.; Tanimoto, S. *Polymer* **2004**, *45*, 7317.
(22) Nojima, S.; Akutsu, Y.; Akaba, M.; Tanimoto, S. *Polymer* **2005**, *46*, 4060.
(23) Hamley, I. W.; Castelletto, V.; Castillo, R. V.; Muller, A. J.; Martin, C. M.; Pollet, E.; Dubois, Ph. *Macromolecules* **2005**, *38*, 463.
(24) Li, W.; Kong, X.; Zhou, E.; Ma, D. *Polymer* **2005**, *46*, 11655.
(25) Radano, C. P.; Scherman, O. A.; Stutzmann, N. S.; Muller, C.; Breiby, D. W.; Smith, P.; Janssen, R. A. J.; Meijer, E. W. *J. Am. Chem. Soc.* **2005**, *127*, 12502.
(26) Hamley, I. W.; Parras, P.; Castelletto, V.; Castillo, R. V.; Muller, A. J.; Pollet, E.; Dubois, P.; Martin, C. M. *Macromol. Chem. Phys.* **2006**, *207*, 941.
(27) Wunderlich, B. *Macromolecular Physics. 3: Crystal Melting*; Acadenic Press: New York, 1980.
(28) Cheng, S. Z. D.; Cao, M. Y.; Wunderlich, B. *Macromolecules* **1986**, *19*, 1868.
(29) Yeh, J. T.; Runt, J. *J. Polym. Sci., Polym. Phys. Ed.* **1989**, *27*, 1543.
(30) Hsiao, B. S.; Gardner, K. H.; Wu, D. Q.; Chu, B. *Polymer* **1993**, *34*, 3996.
(31) Nojima, S.; Kanda, Y.; Sasaki, S. *Polym. J.* **1998**, *30*, 628.
(32) Nojima, S.; Kikuchi, N.; Rohadi, A.; Tanimoto, S.; Sasaki, S. *Macromolecules* **1999**, *32*, 3727.
(33) Nojima, S.; Kato, K.; Yamamoto, S.; Ashida, T. *Macromolecules* **1992**, *25*, 2237.
(34) Nojima, S.; Hashizume, K.; Rohadi, A.; Sasaki, S. *Polymer* **1997**, *38*, 2711.
(35) Sworen, J. C.; Smith, J. A.; Wagener, K. B.; Baugh, L. S.; Rucker, S. P. *J. Am. Chem. Soc.* **2003**, *125*, 2228.
(36) Brandrup, J.; Immergut, E. H. Ed. *Polymer Handbook*, 3rd ed.; Wiley: New York, 1989.
(37) Crescenzi, V.; Manzini, G.; Calzolari, G.; Borri, C. *Eur. Polym. J.* **1972**, *8*, 449.
(38) Nojima, S.; Kato, K.; Ono, M.; Ashida, T. *Macromolecules* **1992**, *25*, 1922.
(39) Stehling, F. C.; Mandelkern, L. *Macromolecules* **1970**, *3*, 242.
(40) Feigin, L. A.; Svergun, D. I. *Structure Analysis by Small-Angle X-ray and Neutron Scattering*; Plenum Press: New York, 1987.
(41) Swan, P. R. *J. Polym. Sci.* **1962**, *56*, 409.
(42) DiMarzio, E. A.; Guttman, C. M.; Hoffman, J. D. *Macromolecules* **1980**, *13*, 1194.
(43) Whitmore, M. D.; Noolandi, J. *Macromolecules* **1988**, *21*, 1482.
(44) Chatani, Y.; Okita, Y.; Tadokoro, H.; Yamashita, Y. *Polym. J.* **1970**, *1*, 555.
(45) Hermans, P. H.; Weidinger, A. *J. Appl. Phys.* **1948**, *19*, 491.

MA0627830